Where and why do creeks evolve on fringing and bare tidal flats?

Hanssen, Jill Leonarda Josepha; van Prooijen, Bram Christiaan; Volp, Nicolette Dominique; de Vet, Paul Lodewijk Maria; Herman, Peter Maria Jozef
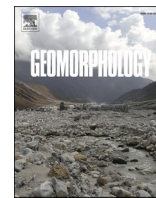
Important note
To cite this publication, please use the final published version (if applicable).
Please check the document version above.

Where and why do creeks evolve on fringing and bare tidal flats?

Jill Leonarda Josepha Hanssen [a,b,*], Bram Christiaan van Prooijen [a], Nicolette Dominique Volp [c],
Paul Lodewijk Maria de Vet [a,b], Peter Maria Jozef Herman [a,b]

[a] *Delft University of Technology, Mekelweg 5, 2628 CD Delft, the Netherlands*
[b] *Deltares, Boussinesweg 1, 2629 HV Delft, the Netherlands*
[c] *Nelen & Schuurmans, Zakkendragershof 34-44, 3511 AE Utrecht, the Netherlands*

ABSTRACT

Although tidal flats appear homogeneous from a distance, morphological variations are found on various spatial scales. These are driven by physical and/or biological processes. In this paper, we consider the creeks that are present on fringing tidal flats and which are orientated approximately perpendicular to the main channel. To explain why these creeks occur, we analysed high-resolution aerial pictures and yearly measured LiDAR data of the Ems-Dollard and Western Scheldt estuaries, located in the Netherlands. We selected nine bare fringing tidal flats, with and without creeks in both estuaries. Subsequently, we related the flat shape to the creek occurrence by evaluating cross-sections of tidal flats from the two estuaries. Finally, we studied how the flat shape affects the cross-shore flow velocity with a 1D numerical model to link creek occurrence to tidal flow. The results show highest ebb velocities, the largest velocity gradients and the largest erosion potential at the transition area between the lower and the upper flat. The milder the slope of the upper flat and the shorter the transition zone, the larger the flow velocities. Based on the data analysis and numerical model outcomes, we conclude that the conditions are favourable for creeks on convex-up intertidal flats with a sharp transition between the upper part and lower part of the flat and that they are predominantly found in this transition zone. We finally argue that these tidal creeks are not only a consequence of the tidal flat profile, but also affect the (equilibrium) profile of the tidal flat.

1. Introduction

Tidal channels and creeks are key elements of estuarine systems and major routes for water discharge and sediment transport. In the branched and interconnected network of channels and creeks, the term 'tidal channel' is usually reserved for the large-scale channels that are continuously submerged, whereas tidal creeks denote the small-scale channels that intersect tidal flats and completely emerge during low tide. Although all estuaries with alluvial beds consist of channels and shoals, not every tidal flat has creeks (Coco et al., 2013; Whitehouse et al., 2000). Knowledge is still limited on which factors determine whether creeks form on tidal flats and where they most likely occur.

Such knowledge of the formation and persistence of tidal creeks contributes to the understanding of the hydrodynamics and morphodynamics of tidal flats (Fagherazzi and Mariotti, 2012; Green and Coco, 2007; Xie et al., 2018). This is crucial information for the preservation of the ecosystem and for flood protection. Creeks may contribute to the

efficient dewatering of the tidal flat (Whitehouse et al., 2000; Zhou et al., 2014), thereby affecting the opportunities for the establishment of diatom mats on the tidal flat and the development of a two-way biogeomorphological interaction (Weerman et al., 2010). Also, creeks can function as an indicator for the flat state. A proper understanding of the links between presence of creeks and tidal flat characteristics like height and shape might be used for predictions of aggradation/degradation of the tidal flat.

Creeks on tidal flats can have their origin in saltmarshes, or they can start on the bare mud flat. In general, they end in a larger channel or creek. A number of studies investigated the relation between creek presence and the flat characteristics, which resulted in empirical formulations, for instance for relations between tidal prism and cross-sectional area of the creek (D'Alpaos et al., 2005, 2010; Marani et al., 2003a, 2003b). However, the focus of these studies was mainly on creeks in marshes and not on bare flats. Erosion of the soil and the resulting creek formation differ between marshes and bare flats, as

vegetation affects flow patterns and strength of the bed. We focus on the bare part of fringing flats (bounded by a channel and a land boundary) and exclude creeks connected to a saltmarsh.

On bare tidal flats, Whitehouse et al. (2000) and Kleinhans et al. (2009) observed creeks near the transition point of convex-up tidal flats in different estuaries. The transition point is defined as the (abrupt) transition in slope between the lower steeper part of the flat and the higher mild-sloped part of the flat. Whitehouse et al. (2000) studied different mudflats in Europe and summarized typical bed forms on bare tidal flats. According to their study, creeks act as a drainage channels for rainwater runoff and dewatering of the upper flat in the late ebb phase. Creeks are created due to the concentrated flow of this retained seawater and rainfall. If there is a local lowering of the bed, more water is attracted which enlarges flow velocities and bed shear stresses. This leads to more erosion at the location of the depression. Hence, a positive feedback establishes. In the surrounding of the depression, the opposite happens: lower flow velocities, resulting in less erosion and a smaller probability of creek formation.

Kleinhans et al. (2009) investigated a tidal flat with several creeks. This fringing tidal flat was situated between a dike at the upper flat and a tidal channel at the lower flat. The upper flat had a milder slope than the lower part of the flat, implying a convex-up profile. They conclude that the creeks are narrow and slightly deeper on the lower and steeper part of the flat. In addition, they found backward eroding steps at this lower part. At the upper flat, near the transition point to the lower flat, the largest creek width and strongest meandering of the creek were found. The creeks became shallower and narrower towards the dike, at the upper boundary of the flat. Kleinhans et al. (2009) relate the difference in creek shape to the tidal flat geometry and ebb flow. Near the transition point, the ebb flow is largest near the transition point for the majority of time, resulting in the most efficient erosion. In flume experiments, Kleinhans et al. (2009) tested the initiation and dynamics of creeks. Only when an initial creek was carved on the bed of the lower flat, a creek developed by eroding backward steps that moved further upstream and deepened the channel.

The development of creeks on bare flats has been investigated with numerical models as well. Xu et al. (2017) modelled the evolution of a network of creeks and the presence of an equilibrium configuration on a convex-up bare flat with a two-dimensional morphological model. The modelled flats initially had a sharp transition point, with a perfectly horizontal upper flat. Creek initiation occurred at the upper flat close to the transition between the upper and lower flat. After initiation, the creeks extended landward and seaward. In these simulations the transition point shifted to a lower point on the vertical axis but the flat shape remained convex-up.

The initiation and equilibrium state of short tidal channels were modelled by Xu et al. (2019). They used a quasi 2D morphodynamic model. The initial flats were horizontal and the elevation was below the low waterline. In time the landward part of the flats accreted faster, resulting in a sloped profile. The change in geometry resulted in a cross-shore gradient in the discharge and bottom shear stresses. Due to erosion, creeks were initiated at the seaward boundary of the model and grew landward.

The observational, experimental and model studies discussed have several conclusions in common. Creeks were observed on convex-up flats and they were most prominent on the upper flat near the transition between lower and upper flat. Flume experiments and numerical models (Kleinhans et al., 2009 and Xu et al., 2019, respectively) suggest that creeks are formed on the lower flat. In the experiment it is not stated explicitly if creeks grew from the lower flat to the upper flat. In the model study, creeks did not grow from the lower flat over the transition point towards the upper flat. This seems to be contradicted by observations. Neither experiments nor modelling fully resolve the conditions for creek establishment on convex-up tidal flats. Neither do they explain why some convex-up tidal flats have no creeks at all.

In this paper, we aim to answer the main research question: Where and why do creeks occur on bare tidal flats. Answering this question will contribute to intriguing questions that are of direct relevance for managing tidal flat systems. The first question is: Are creeks of influence on the stability of tidal flats? This would imply a feedback mechanism between small scale morphology and large scale morphology. The second question is: Can creeks be used as indicators for the tidal flat morphology? This would make it possible to deduce tidal flat morphology information from satellite images.

We analysed bathymetric data of flats in two estuaries to identify where creeks occur and to derive the flat shape characteristics. Based on the literature we assume that creeks develop due to erosion of the tidal flat. We investigated the erosion probability of a tidal flat for tidal flow conditions with a one-dimensional hydrodynamic numerical model for a range of profiles. The outcomes are combined to a conceptual framework indicating where and why creeks occur on tidal flats.

This paper is structured as follows. In the Methods section, an area description is given of the research locations; the LiDAR data processing is described and the numerical model is explained. In the Results section, we present our findings of the data analysis and identify the locations of creeks. Furthermore, tidal flat characteristics, such as bed slope and height, are determined. The cross-shore flow velocities and erosion potential are presented, extracted from the numerical model. In the Discussion section, we compare the findings of the spatial analyses and the modelling and compare them to existing literature. Furthermore, we discuss the impact of creeks intersecting a bare tidal flat.

2. Methods

2.1. Research locations

We selected tidal flats in the estuaries Ems-Dollard (north-western part of the Netherlands) and Western Scheldt (south-western part of the Netherlands), see Fig. 1. Different types of tidal flats are present in both estuaries, ranging from intertidal shoals surrounded by channels to fringing tidal flats bounded by a dike and a channel. In order to focus on the processes in cross-shore direction, we only selected bare fringing flats, situated between a dike (or saltmarsh) on the upper part and a channel at the lower end.

The **Ems-Dollard** is located in the northeast of the Netherlands at the border with Germany. The estuary is 50 km long and connected upstream to the Ems River (Germany) and downstream to the Wadden Sea. The yearly average fresh water discharge from the Ems River is 100 m^3s^{-1} (Compton et al., 2017a). This estuary is tide dominated and the tidal range varies from 2.3 m at the mouth of the estuary to 3.2 m in the southern part. The maximum current velocities are 1.5 ms^{-1} in the main channel (Herrling et al., 2014). The maximum depth equals 30 m (Compton et al., 2017b; Talke et al., 2009). Half of the estuary consists of intertidal areas (141 km^2) (Compton et al., 2017b). The tidal flats in the Ems-Dollard are built up by fine sediments. Grainsizes (d_{50}) between 7 and 10 μm on different tidal flats throughout the estuary where measured (DINOloket).

The **Western Scheldt**, located in the southwest of the Netherlands, is the downstream part of the River Scheldt. The estuary is 55 km long and ranges from the border with Belgium (near WS-Bath) to the North Sea. The estuary is a macro-tidal system and the tide dominates the river discharge, which is 100 m^3s^{-1} on average (van der Wegen and Roelvink, 2012). The tidal range is amplified in the funnel-shape from 3.5 m near the mouth to 5.2 m near WS-Bath and the maximum current velocities exceed 1 ms^{-1} for an average tide (de Vet et al., 2017; Wang et al., 2019). The estuary is a multi-channel system with intertidal flats between and along the channels. The maximum depth equals 45 m (Dam et al., 2013). The intertidal area amounts to 90 km^2, which is 30% of the total surface area of the basin (Stark et al., 2017). Dredging activities intensified the tidal amplification (van der Wegen and Roelvink, 2012) and led to morphological changes of the tidal flats in the Western Scheldt (de Vet et al., 2017, 2020). Many fringing tidal flats are present along
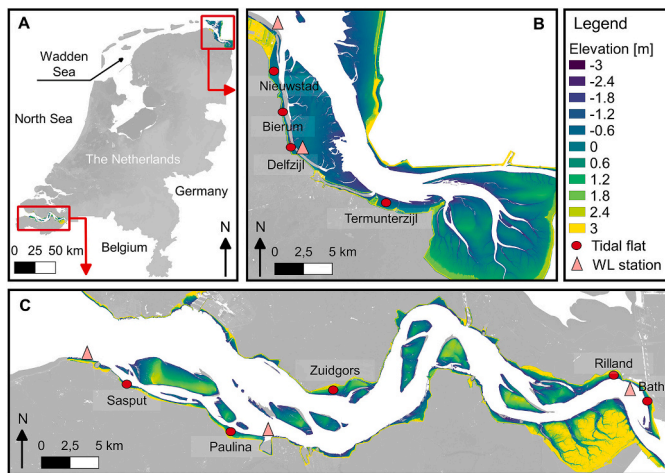
Fig. 1. A) The Netherlands and locations of the Western Scheldt and Ems-Dollard. B) Selected tidal flats Ems-Dollard. Only ED-Termunterzijl is not covered with creeks. C) Selected tidal flats Western Scheldt, tidal flat WS-Rilland is not covered with creeks. In all tree maps, the colored area indicates the elevation (LiDAR data 2014) of the intertidal zone. The pink triangles indicate the water level measurement stations.

the borders of the estuary. These fringing flats are characterized by typical grain size ranges between 20 and 150 μm (de Vet et al., 2017; Willemsen et al., 2018; Zhu et al., 2019) and host a variety of benthic species (Ysebaert et al., 2003).

2.2. Spatial analyses

2.2.1. Data sets Ems-Dollard

Aerial pictures and satellite images were used to identify tidal flats with and without creeks. For the Ems-Dollard we used satellite images of the Google Earth Pro application with a resolution up to 10 m × 10 m (Google Earth Pro, 2016). The Dutch authorities gathered bathymetry maps of the tidal flats in the Ems-Dollard. The bathymetry data contains LiDAR measurements (RWS, 2014). These are Digital Elevation Maps (DEM) obtained by laser altimetry. In this estuary the LiDAR is obtained once in the five years. In the current study, LiDAR data of 2014 were considered, as both estuaries were measured that year with LiDAR at a resolution of 2 m^2.

The Dutch authorities measure the water levels at different locations in the Ems-Dollard every 10 min. We selected two measurement stations closest to the relevant tidal flats (Fig. 1) and used the 10 min measurements of the year 2014 (RWS Waterinfo, 2014). First, we removed the invalid measurement points from the data set. Then, we calculated the mean water level (MWL) by averaging all water level measurements. For each tidal cycle we filtered the maximum (minimum) water level and we averaged these values to obtain the mean high water level, MHWL (mean low water level, MLWL). Based on these values, the tidal range was determined by the difference between MHWL and MLWL.

2.2.2. Data sets Western Scheldt

The aerial pictures of the Western Scheldt (Province of Zeeland, 2014) have a resolution up to 0.25 m × 0.25 m and are taken yearly by the Dutch authorities. The Dutch authorities have measured the tidal flats in the Western Scheldt extensively and the LiDAR data are collected yearly in this estuary. The spatial resolution of the LiDAR data increased from 5 m^2 to 2 m^2 in the last decade.

We used the water level measurements of three measurement-stations in the Western Scheldt (Fig. 1) to calculate the MHWL, MWL and MLWL of the year 2014. The measurement frequency of the stations is 1/10 min and we used the same filter procedure as we did for the Ems-Dollard. All data types with measurement resolution and frequency are

Table 1
Overview of used data sets to extract tidal flat bathymetries, creek presence and tidal elevations. For each data set the location, source, measurement resolution and measurement frequency is included.

Data type	Meta data	Ems-Dollard	Western Scheldt
Aerial pictures	Resolution	10 m × 10 m	0.25 m × 0.25 m
	Frequency		1/ year
	Source	Google Earth Pro, 2016	Province of Zeeland, 2014
LiDAR	Resolution	2 m × 2 m	2 m × 2 m
	Frequency	1/ 5 year	1/ year
	Source	RWS, 2014	RWS, 2014
Water levels	Resolution	0.01 m	0.01 m
	Frequency	1/ 10 min	1/ 10 min
	Source	RWS Waterinfo, 2014	RWS Waterinfo, 2014

summarized in Table 1.

2.2.3. Tidal flat selection

We observe flats with and without creeks at different locations throughout each estuary. This is observed despite the fact that in both estuaries the range of the tidal amplitude varies. Only flats with a minimum cross-shore width of 100 m are considered. The boundary was set at a marsh edge or at a dike, whatever was present. In long-shore direction we selected tidal flats of a minimum length of 100 m. Moreover, flats that are located near a channel bend or near a hydraulic
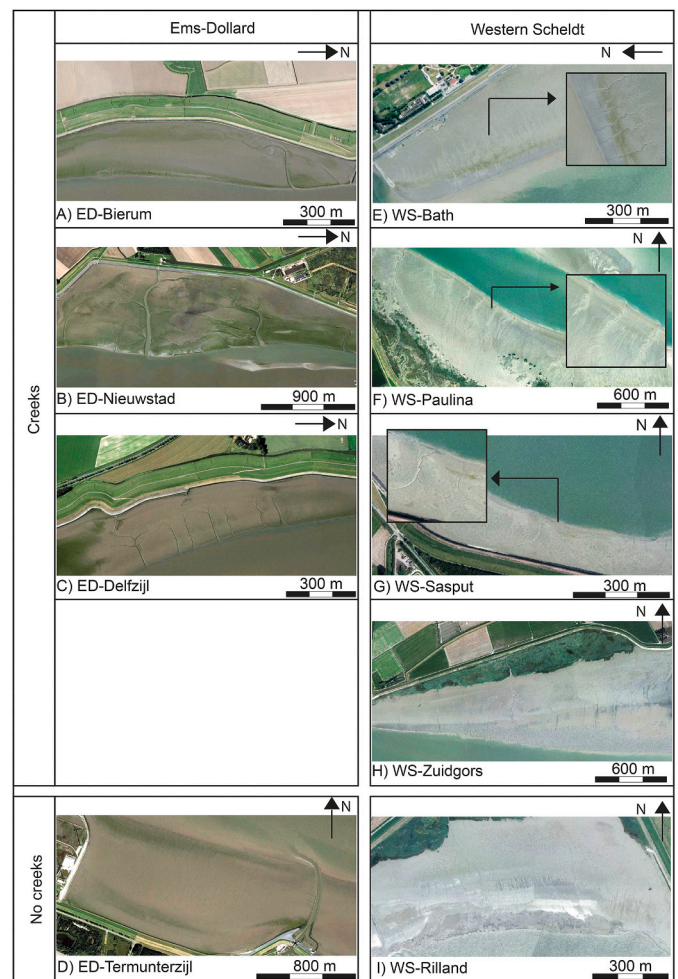
Fig. 2. Aerial images of the selected tidal flats with and without creeks. Panels A-D: Ems-Dollard (Google Earth Pro, 2016). Panels E-I: Western Scheldt(Province of Zeeland (2014). The scale varies and is indicated with the scale bar.

structure were excluded. This to focus on the natural behaviour.

To distinguish flats with and without creeks, we inspected the aerial pictures. For the flats with creeks, we only selected flats where at least one creek was not connected with either a marsh or a freshwater outlet from the hinterland. Minor creeks, below the LiDAR data resolution, are not considered.

In total we investigated nine different tidal flats in both estuaries. In the Western Scheldt, we selected four tidal flats with and one tidal flat without creeks. In the Ems-Dollard, three tidal flats with and one tidal flat without tidal creeks were selected. The locations are indicated in Fig. 1. For each flat the presence or absence of creeks, the distance between creeks and the flat width were identified and qualified.

To illustrate the creek presence of the locations indicated in Fig. 1B and C, we present the aerial pictures of the selected tidal flats in the Ems-Dollard and Western Scheldt in Fig. 2. Note that the scale varies between images. In the Ems-Dollard, the flats close to ED-Bierum, Niewstad and ED-Delfzijl have distinct creeks (Fig. 2A-C, respectively). At ED-Bierum there is only one creek, at ED-Nieuwstad and ED-Delfzijl there are multiple creeks. The large creek in the middle of the flat Nieuwstad developed due to an outfall. At ED-Delfzijl, we see a pattern of creeks. No creeks are found at the tidal flat of ED-Termunterzijl (Fig. 2D).

For the Western Scheldt, creeks are present at the tidal flats of WS-Bath, WS-Sasput and WS-Paulina creeks are present (Fig. 2E-G, respectively). These creeks do not have a connection with the marsh. At WS-Bath there is a pattern of multiple tidal creeks. Further to the right in the picture these vanish. Also at WS-Paulina, we observe a pattern of creeks. At the tidal flat of WS-Zuidgors (Fig. 2H), there are three creeks that flow from the marsh over the tidal flat. Furthermore, we observe mature creeks that vanish in some years. At the tidal flat of WS-Rilland, we do not observe creeks (Fig. 2I). Compared to the Ems-Dollard, the creeks of the Western Scheldt are shorter and narrower. Probably the creeks are shallower too, but that cannot be derived from the LIDAR data.

2.2.4. Analysis protocol

The LiDAR data were analysed with the geographical information system QGIS (QGIS.org, 2021). The DEM contained elevations on a grid of XY coordinates (EPSG: 28992 reference system). Cross-sections were drawn perpendicular to the MWL contour line of each tidal flat. If creeks were present, the cross-section was taken close to the creek. Those cross-sections did not intersect the creek to ensure that the cross-section was representative for the flat. The elevation points of the grid cells that intersect with the cross-sections were interpolated to this cross-section. The interpolated points had an equally spaced intervals between 2 and

2.8 m, depending on the angle between the grid and the cross-section.

These cross-sections (profiles) were smoothed with the LOWESS method, to compute the slope of the tidal flat robustly without the local irregularities. This method is a weighted moving regression method to re-evaluate the value of each point of the profile. Each data point A and its neighbouring data points (defined with a sliding window) is a subset of the data. A polynomial is fitted to this subset to re-evaluate the value of point A. Data points closer to point A have a higher weight to determine the shape of the polynomial and the value of A (*Cleveland and Devlin 1988*).

Fig. 3A, presents the cross-section of a tidal flat. The grey stars represent the raw data points, the black solid line is the smoothed data. Fig. 3B presents the bed slope in cross-shore direction based on the smoothed data, the black solid line. To characterize the profiles with a limited set of parameters, we defined a double-sloped profile, with a transition zone in between. The flats consist of a lower flat and its slope is called S_{low} [−], and an upper flat with a (relatively) milder slope, S_{up} [−]. The two slopes are connected via a transition zone with length scale δ [m]. The bed slope can therefore be described by the function:

$$s = \frac{1}{2}\left(S_{low} - S_{up}\right)\left(1 - tanh\left(\frac{x-L}{\delta}\right)\right) + S_{up},\tag{1}$$

with x [m] the horizontal coordinate, perpendicular to the tidal channel and L [m] the horizontal position of the transition point of the slope. The function in Eq. (1) was fitted with a least square error method to the first order derivative of the data (Fig. 3B, red line). From this fit we obtained the mean values and standard deviations of S_{low}, S_{up}, L and δ.

By integrating Eq. (1) over x, we obtain the expression for the bed level:

$$z_b = z_0 + \frac{1}{2}\left(S_{low} - S_{up}\right)\delta\left[\frac{x-L}{\delta} - log\left(cosh\left(\frac{x-L}{\delta}\right)\right) - log(2)\right] + S_{up}(x-L),$$
$$\tag{2}$$

the height z_0 [m] is defined as the position of the transition point of the two slopes when extrapolating the two slopes into the transition zone (blue dotted lines in Fig. 3A).

Second, we fitted Eq. (2) to the smoothed data. The mean values obtained from the fit with Eq. (1) were used as initial parameters for the fit with Eq. (2). We found the mean and standard deviations of z_0, S_{low}, S_{up}, L and δ of Eq. (2) (Fig. 3A, red line). z_0[m] is the vertical shift of the profile to obtain the actual bed height of the existing flats.

2.3. Model description

We investigated the flow velocities in cross-shore direction with a 1D model for different flat profiles. Furthermore, we used a geometrical model to interpret the model results in more detail.

2.3.1. Numerical model

The 1DH model (uniform in width and over depth) is based on Volp et al. (2013). This finite volume based model automatically deals with flooding and drying, see also Casulli (2009). With this approach we do not have to consider a flooding threshold. This is very favourable when modelling the shallow water flows over a tidal flat. The model uses a staggered grid; the water levels are defined in the cell centres, and the velocity and discharge are defined at the edges of a grid cell. Information of the bed level is available in the centres and on the edges of the cell.

The model solves the 1D shallow water equations (1D SWE): it combines the conservation of volume (Eq. (3)) with an equation of momentum (Eq. (4)). In the equation of momentum, the change in velocity (left-hand side) is caused by advection, inertia, pressure and the bed friction.
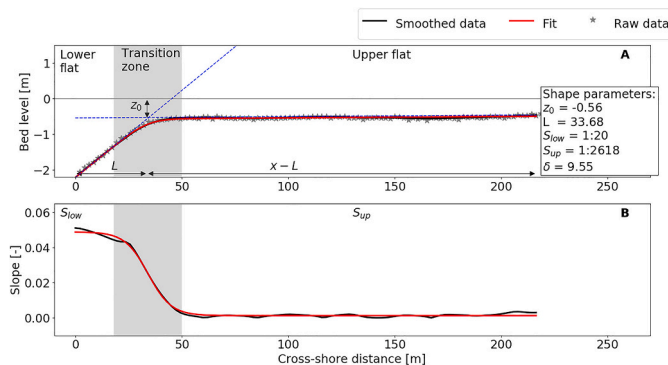
Fig. 3. A) Example of fitting Eq. (2) (red) to the smoothed bed level data (black) of a cross-section. The blue lines are the extrapolated slopes, z_0[m] is the vertical shift of the intersection of both slopes. L [m] is the length of the lower flat when it is extrapolated into the transition zone. The grey zone is the transition zone with length scale δ. B) fit of Eq. (1) (red) to the slope of the smoothed data (black) and the slope of the lower flat, S_{low}, and the upper flat S_{up}.

$$\frac{dV(\eta)}{dt} = (ud)_{out} - (ud)_{in},\tag{3}$$

$$\frac{\partial u}{\partial t} = -u\frac{\partial u}{\partial x} - g\frac{\partial \eta}{\partial x} - \frac{g|u|}{C^2 d}u, \tag{4}$$

With water level η [m]; water depth d [m]; flow velocity u [ms^{-1}]; gravitational acceleration g [ms^{-2}]. The friction term is a function of the Chézy coefficient, C [m$^{1/2}$s^{-1}], which is defined as:

$$C = 18log\left(\frac{12d}{k_s}\right), \tag{5}$$

with roughness height k_s [m]. We refer to Volp et al. (2013) for further details of the numerical solution techniques.

2.3.2. Model settings

In each simulation we used a grid size of 3 m Because the spacing between the grid points in the measured profile is 2.8 m, a higher resolution is not needed. With a lower resolution we lose information about the flow velocity, especially in the transition zone. We did not expect that the flow velocity would exceed 1 m/s based on measured flow velocities in the Western Scheldt (e.g. Zhu et al., 2019). We used a time step of 2 s, to meet the numerical requirements. We focussed on the hydrodynamic tidal forcing and used the tidal cycle that is present in both estuaries 12.4 h). A typical value of $k_s = 0.02$ m was chosen. Applicable values for the Chézy factor range between 45 and 65 m$^{1/2}$s^{-1} (van der Wegen et al., 2017; Volp et al., 2013). To avoid unrealistic values for small water depths, the Chézy factor is set to a minimum value of 30 m$^{1/2}$s^{-1}.

We focussed on fringing bare flats between the tidal channel and a marsh edge or dike. In the model, the dike or marsh edge is a closed boundary whereas water level boundary condition is imposed at the tidal channel. A sinusoidal water level boundary is imposed by

$$\eta = \eta_0 + a_{M2}cos\left(2\frac{\pi}{T}t\right), \tag{6}$$

with η_0 [m] the mean water level (MWL); tidal amplitude a_{M2} [m]; tidal period T [s] and time t [s]. The MWL and amplitude depend on the flat location and can be found in Table 2. In the post processing, we averaged the flow velocities of the model runs in bins of 12 min and the flow velocity was set to zero for water depths smaller than k_s.

We investigated profiles with and without creeks. For each estuary we selected and modelled one profile of each type. In both estuaries there was only one flat without creeks that complied with the selection criteria. For the flats with creeks we selected a tidal flat that was representative for all tidal flats with creeks in the estuary. We explored if there were significant differences in flow velocities over the four different tidal flats with the model. In addition, we studied the effect of the flat shape on the flow velocities over the flat with a theoretical flat
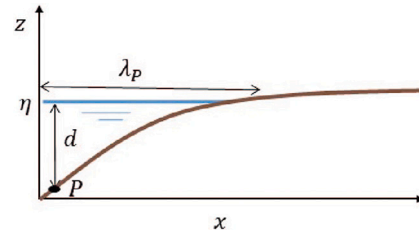

Fig. 4. Schematisation of the cross-section of a tidal flat with observation point P at time step t (related to Eq. (9)). η is the water level, d is the water depth in P and λ_P the length of the water volume in P. x is the cross-shore coordinate and z the vertical coordinate.

profile based on Eq. (2) (simulation Base case) and adjusted the upper and lower slopes (S_{low} and S_{up}, respectively) and curvature (δ) of this flat. In total we modelled eight idealised profiles. An overview of all simulations and flat characteristics is presented in Table 2.

2.3.3. Geometrical approach

We used an analytical model to gain more insight in the model results. The analytical expression is based on the continuity equation in combination with a rigid lid (the water level is uniform at every time step), see also van der Wegen et al. (2019). This approach neglects the momentum equation and thereby the dynamics caused by advection and bed friction. This can only be used in a 1D setting. At location x_p (Fig. 4) we can define the discharge q at time t by:

$$q(x_p, t) = u(x_p, t)d(x_p, t), \tag{7}$$

with q [m^{2}s^{-1}] as the discharge per unit width and depth $d = \eta - z_b$ [m], with water level η and bed level z_b. Applying the continuity equation and the rigid lid assumption we obtain:

$$q(x_p, t) = \frac{d\eta(t)}{dt}\lambda_p(x_p, t), \tag{8}$$

With λ_p [m] as the length of the water line from position P: $\lambda_p = x(z_b = \eta) - x_p$ (see Fig. 4).

Combining Eqs. (7) and (8) results in the velocity:

$$u(x_p, t) = \frac{d\eta}{dt}\frac{\lambda_p}{d}, \tag{9}$$

The velocity can now be determined at every position for a given water level time series $\eta(t)$ and a continuously increasing bed level. We limited d to 0.01 m to avoid unrealistic flow velocities. For a given tidal forcing, the analytical model directly links velocity to the geometry of the domain.

Table 2
Properties and input parameters of modelled flats. The first four profiles are based on actual bathymetries from the Ems-Dollard (ED) and the Western Scheldt (WS). The Base case (fifth row) profile is an idealised bathymetry based on results from the observed data. Profiles 6–11 are variations of the Base case. Columns 1–9 provide information about the flat characteristics. The high water (HWL), mean water (MWL) and low water (LWL) as used in the model is included in columns 10–12.

Est.	Name	Creeks present along profile	Total length [m]	Length lower flat [m]	Length upper flat [m]	S_{low} Slope lower flat [−]	S_{up} Slope upper flat [−]	Delta [m]	LWL [m]	MWL [m]	HWL [m]
ED	Delfzijl 1	Yes	216	34	183	1:20	1:2617	10	−1.3	0.1	1.
ED	Termunterzijl 1	No	797	0	797	1:67	1:680	203	−1.3	0.1	1.5
WS	Paulina 2	Yes	429	24	405	1:18	1:588	30	−2.0	0.2	2.4
WS	Rilland 1	No	461	188	273	1:63	1:444	77	−2.5	0.2	2.9
–	Base case	–	600	100	500	1:40	1:1000	40	−2.5	0.0	2.5
–	S_{low} - 1	–	600	100	500	1:20	1:1000	40	−2.5	0.0	2.5
–	S_{low} - 2	–	600	100	500	1:80	1:1000	40	−2.5	0.0	2.5
–	S_{up} - 1	–	600	100	500	1:40	1:500	40	−2.5	0.0	2.5
–	S_{up} - 2	–	600	100	500	1:40	1:2000	40	−2.5	0.0	2.5
–	δ - 1	–	600	100	500	1:40	1:1000	10	−2.5	0.0	2.5
–	δ - 2	–	600	100	500	1:40	1:1000	160	−2.5	0.0	2.5
–	Concave-up	–	600	500	100	1:1000	1:40	40	−2.5	0.0	2.5

2.3.4. Erosion potential

With the numerical model we evaluated the impact of the flow on the mobilization of sediment from the bed. To this end, we defined the erosion potential S [kg m^{-2}] as the integrated erosion over a tidal cycle:

$$S = \int_0^T E(t)dt, \tag{10}$$

with erosion rate E [kg m^{-2} s^{-1}]. The erosion potential indicates how much erosion could take place during a tidal cycle. Although there is a variety of erosion rate formulations, all have the form of

$$E = M\left(\frac{\tau_b - \tau_{cr}}{\tau_{cr}}\right)^n, \tag{11}$$

for $\tau_b > \tau_{cr}$ and erosion rate coefficient M [kg m^{-2} s^{-1}], bed shear stress τ_b [Nm^{-2}], critical bed shear stress for erosion a τ_{cr} [Nm^{-2}] and coefficient n. Following the Partheniades erosion rate formulation for fine sediment (Winterwerp and Van Kesteren, 2004), we assume $n = 1$. The flow-induced bed shear stress in cross-shore direction is defined by

$$\tau_b(t) = c_f \, \rho_w \, u(t)^2, \tag{12}$$

with skin friction c_f [−], density of water ρ_w [kg m^{-3}], and depth-averaged flow velocity u [ms^{-1}]. The flow velocity follows from the numerical simulations. The skin friction is set to a typical value of c_f=0.003 which is consistent with a Chézy value of 57.18 [m$^{1/2}$s^{-1}]; the density of water to ρ_w=1000 kg m^{-3}; the critical bed shear stress to τ_{cr}=0.1 Nm^{-2}; and erosion rate coefficient to M= of $0.2 \cdot 10^{-3}$ kg m^{-2}s^{-1} (Winterwerp and Van Kesteren, 2004).

3. Results

3.1. Field data: spatial characteristics

The cross-shore tidal flat shape is a potential indicator for creeks in both estuaries. To investigate whether the shape of a tidal flat relates to the occurrence of creeks, cross-sections and the zones covered by creeks are presented for nine flats in Fig. 5. At least two cross-sections (black solid lines) are plotted per flat. The fit of Eq. (2) is plotted by dashed lines for each cross-section. The fitting parameters are given in Appendix A. The grey area indicates the zone where creeks cut through the tidal
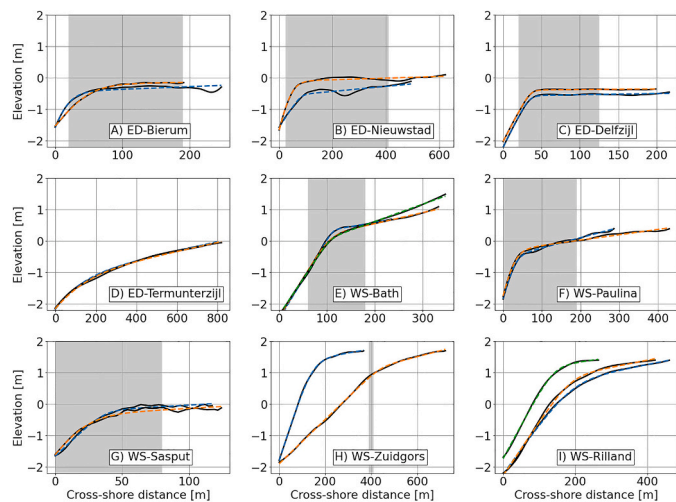

Fig. 6. Comparison of flat parameters. Relation between the absolute value of z_0 and the curvature. The shape of the marker relates to the tidal flat, the colour to the transect of each flat. The markers with the red edges belong to flats without creeks; WS-Rilland and ED-Termunterzijl.

flat. Creeks on a single flat differed in length; the grey zone covers the maximum creek length.

The replicate cross-sections of a single flat had a similar shape in the Ems-Dollard. All flats, except the flat at ED-Termunterzijl, had a distinct transition point (Fig. 5D). The flat at ED-Termunterzijl showed no creeks, in contrast to all other flats. The tidal flat of ED-Delfzijl (Fig. 5C) had a significantly smaller upper slope (S_{up}) and smaller transition length (δ) compared to the other two flats with creeks. Furthermore, a higher density of smaller creeks was observed at ED-Delfzijl.

At each of the sites in the Western Scheldt, cross-sections within a specific flat had a similar shape. The flats of WS-Bath, WS-Sasput, and WS-Paulina (Fig. 5E-G, respectively) had creeks and were characterized by a small transition length (δ). The transition point of those flats was below or close to the MWL (0.0–0.2 m). The tidal flat WS-Bath was intersected by numerous creeks with a small spacing (20–50 m). The creeks on this flat were narrower and shorter than those on the other Western Scheldt flats. Within the studied Western Scheldt flats, the flat at WS-Bath had the steepest upper slope (S_{up}) and the smallest transition length (δ). The transition point at WS-Rilland (Fig. 5I) was above MWL. This flat had no creeks. At WS-Zuidgors (Fig. 5H), we observed creeks on the aerial pictures and LiDAR data, but the profile parameters were comparable to the parameters of the creek-less flat at WS-Rilland (see also Fig. 6).

We compared the average values of the flat parameters for flats with and without creeks in both estuaries to unravel systematic differences (Table 3). In the Ems-Dollard flats with creeks had a milder upper slope. In the Western Scheldt this was not the case. In both estuaries the lower slope was slightly steeper and the length of the curved zone smaller for flats with creeks.

We investigated possible relations between the different flat parameters of each transect and the occurrence of creeks. Flats with tidal creeks have a short transition zone δ and the vertical distance z_0 between the transition point and mean sea level (MSL) is small (Fig. 6). We used the absolute value of z_0, because the transition point of the flat can be above or below MSL. Profiles with a small negative or positive value, have a transition point close to the MWL. The markers with the red edges

Fig. 5. Cross-sections of the nine tidal flats A-D located in the Ems-Dollard (ED). E-I located in the Western Scheldt (WS). For every tidal flat 2–3 cross-sections were taken (black solid lines) including the fit with Eq. (2) (dashed lines). The zone where creeks intersect the flat is indicated in grey. The flats ED-Termunterzijl and WS-Rilland are not intersected by creeks. On the vertical axis the elevation is w.r.t. MSL. Note that the horizontal scale varies.
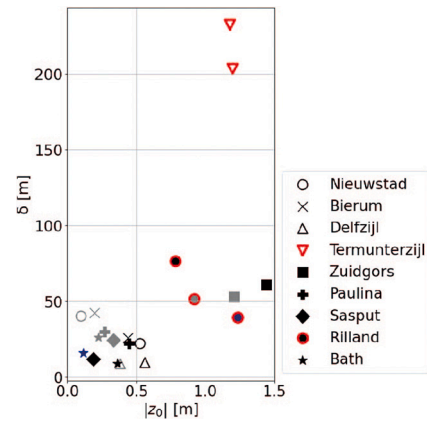
Table 3
Average profile parameters for flats with and without creeks per estuary.

	Ems-Dollard		Western Scheldt	
	Creeks	No Creeks	Creeks	No creeks
S_{low} [−]	1: 24	1: 69	1: 30	1: 55
S_{up} [−]	1: 2119	1: 690	1: 365	1: 500
δ [m]	25	218	27	121

belong to flats without creeks; WS-Rilland and ED-Termunterzijl. For the tidal flats with creeks ($z_0 < 0.6$ m deviation from MWL) and had a relatively small (<50 m) transition length δ. The tidal flat WS-Zuidgors was the exception, which corresponds to the observations of the cross-shore shape.

3.2. Modelling

By means of modelling, we provide insights on how the geometry of a flat and the physical conditions affect the flow velocities across tidal flats and with that the potential for creeks. We studied the cross-shore velocity with the analytical model (geometrical considerations) and the numerical model (physical conditions). To this end, we introduced a Base case simulation of a tidal flat of which the shape parameters were derived from average values of the analysed tidal flats (Table 2).

3.2.1. Analytical model

With the analytical model we isolate the geometric conditions (i.e., the geometric concept Especially a local maximum and the gradient in velocity may explain the occurrence of creeks. There are two factors that determine the maximum velocity in a point x_p, see Eq. (9). The first is the rate of change of the tidal level: $\frac{\partial \eta}{\partial t}$. It is prescribed as uniform over space. The sinusoidal boundary condition implies that it is maximum for mean water level and zero for low and high water. The second factor is the ratio between the length of the hinterland and the depth: $\frac{\lambda_p}{d}$ (where d > 0.01 m to avoid unrealistic values for the flow velocity). This ratio is uniform for linear profiles, increases landwards for convex-up profiles and decreases landwards for concave-up profiles. See also Fig. 7A, presents the flat and observation points of the analytical model. In addition, near the upper point of the upper slope, λ_p is quickly arrested by the dike and does not increase anymore with increasing water levels as soon as the water has reached the foot of the dike. These factors explain the pattern of the velocity as one goes from high water to low water in Fig. 7B. Starting with high water and a zero velocity, the velocity increases for all observation points due to an increase of $\frac{\partial \eta}{\partial t}$. As soon as the water level reaches the toe of the dike, the flow velocities become uniform over the linearly sloping upper profile ($180 m < x < 600 m$).

Around the transition point, the ratio $\frac{\lambda_p}{d}$ at small water depths decreases and the maximum velocity decreases, despite the maximum values for $\frac{\partial \eta}{\partial t}$ in this zone. Over the nearly-linear lower slope, the maximum velocity is determined by the inverse of the lower slope, and as this slope is steeper, the maximum velocity is lower. The flood phase is symmetrical to the ebb phase, as the water level is considered uniform.

3.2.2. Numerical model

With the numerical model we investigated the effect of bed friction, advection and inertia on the flow velocity. Hence, by comparing the results of both models we can distinguish between the effects of the geometry and momentum.

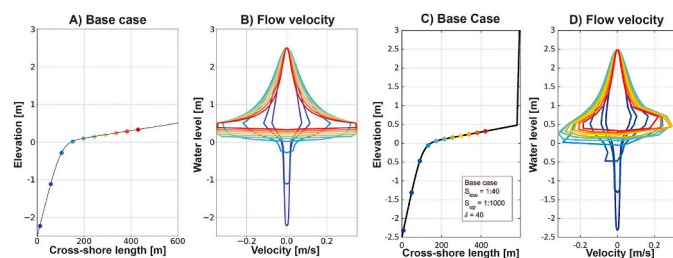Even with the full momentum equation included, the flow velocities as computed with the numerical model are still largely dominated by the geometry of the flat. This implies that the flow velocities follow a similar general pattern (Fig. 7C and D). We determined the leading order terms of the momentum equation based on a scalar approximation like applied by (Friedrichs and Madsen, 1992). In particular the inclusion of friction imposes an essential difference on the velocity. During ebb flow (negative flow velocities in Fig. 7D) maximum flow velocity increases towards the transition point ($x = 180 m$) where it attains its highest values. This contrasts with the nearly-uniform maximum ebb flows on the upper flat derived from geometrical principles in the analytical model. This friction-induced difference is much larger during ebb flow than during flood flow, leading to an asymmetrical pattern. Peak velocities predicted by the numerical model are smaller than those predicted by the analytical model, also as a which is another consequence of bed friction.

In the numerical computation the friction term becomes important for small water depths. The waterline in cross-shore direction differs significantly between ebb and flood for a similar water level at the transition point (Fig. 8). Due to friction, the dewatering of the flat is delayed on the upper flat during ebb. Consequently, a negative water level slope develops (higher on the upper flat compared to the lower flat). This strong gradient is reversed, over a much shorter spatial interval, during flood. In addition, during ebb when the water line reaches MWL, we observe small water depths on the upper flat near the transition point. The shallow water depth results in relatively high flow velocities (as follows from the continuity equation). In this zone the velocities are higher during ebb compared to flood. In the analytical solution there is no delayed dewatering due to the rigid lid approximation (absence of momentum).

From the geometrical considerations in the analytical model we conclude that the upper slope of the flat and the extent of the transition zone are important determinants of the potential maximum velocities near the transition point. A mild upper flat (large value $\frac{\lambda_p}{d}$) and a small inflection zone (fast transition to maximum $\frac{\lambda_p}{d}$), results in higher flow velocities. Accounting for friction in the numerical model introduces an asymmetry between flood and ebb flow, as well as a local maximum peak flow velocity just landwards of the transition point.

3.2.3. Selected flats

To further investigate whether the shape-induced velocities may

Fig. 7. Results of analytical solution (A and B) and numerical model (C and D). Panel A and C) flat profile with observation points. Panel B and D) velocity profile in each observation point. Colour codes correspond to the observation points.
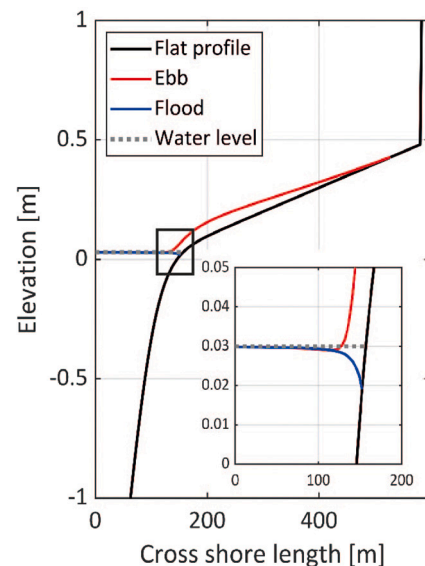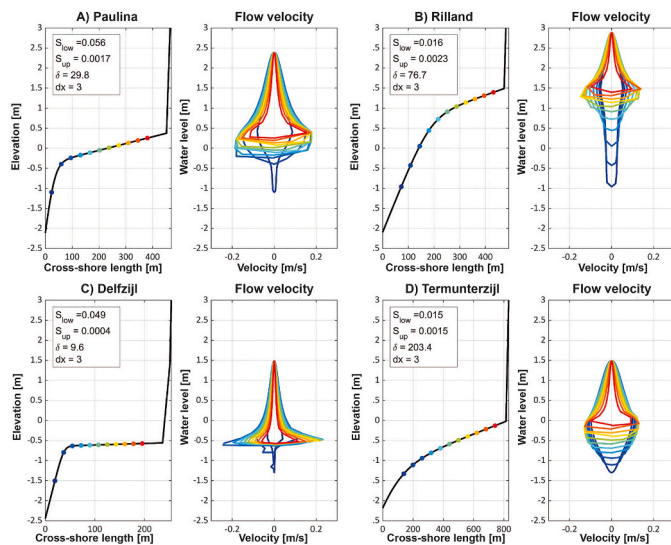
Fig. 8. Comparison of the spatial variation in water line for an equal water level at the boundary for ebb (red) and flood (blue). A spatially constant water line is illustrated with the grey dotted line.

Fig. 9. Cross-shore flow velocity over four tidal flats based on the numerical model. Western Scheldt - creeks: WS-Paulina(A), Western Scheldt - no creeks: WS-Rilland (B). Ems-Dollard – creeks: ED-Delfzijl (C), Ems-Dollard – no creeks: ED-Termunterzijl. (D). In each panel the cross-section (left) and cross-shore velocity profile per observation point (right) are given. The colours of the observation points coincide with the colours of the velocity profiles. We plotted the velocity signals of locations where the change in flow velocity is most distinct. The y-axis are w.r.t. MSL.

explain the occurrence of creeks, cross-shore flow velocities were calculated for one flat with and one flat without creeks in each estuary (Fig. 9). We plotted the bed level and measurement points (panels left hand side) and the flow velocity and water level in the velocity points during the whole tidal cycle (panels right hand side).

The flat profiles of WS-Paulina and ED-Delfzijl (Fig. 9A and C) are both intersected by creeks and have a distinct change in the bed slope, in line with the Base case. Hence, the resulting velocity profiles are comparable to the results discussed in the previous section. In the velocity profiles we observe a sharp gradient, acceleration and deceleration of the flow, for the locations near the transition point and on the upper flat during ebb and flood. The points closest to the transition point are longest exposed to high flow velocities.

The mild upper slope pre-dominantly influences the velocity profiles. This is highlighted by comparing the two cross-sections and the resulting velocity profiles. The transition point of WS-Paulina is closer to the MWL (z_0 0.6 m ED-Delfzijl, 0.5 m WS-Paulina). The slope of the upper flat of WS-Paulina is steeper, resulting in a height of the flat which is about 1.0 m higher in the tidal window compared to that of the profile at ED-Delfzijl. Furthermore, the upper flat of WS-Paulina is 220 m longer. The lower flat of WS-Paulina has a slightly smaller slope.

Although the upper flat of WS-Paulina is longer (more water flows over the transition point), the transition point is closer to the MWL, and the tidal amplitude is larger, the milder slope of ED-Delfzijl dominates those other factors and results in larger flow velocities. The maximum flow velocities for the flat of ED-Delfzijl are higher compared to WS-Paulina (0.25 ms^{-1} and 0.19 ms^{-1}, respectively).

The flow velocity on the upper flat of ED-Delfzijl is higher during flood than during ebb. The very mild slope (almost horizontal bed) results in sudden filling during flood. During ebb, bed friction results in a delay of the dewatering. The closer to the transition point the larger the ebb velocity.

Tidal flats without creeks have a more gradual change in slope of the bed profile, examples are ED-Termunterzijl and WS-Rilland (Fig. 9B and D). The flow velocities are significantly smaller on these tidal flats with a steeper upper slope and a transition point that is a high or low in the tidal window. Consistent with the flats of WS-Paulina and ED-Delfzijl,

Table 4
Summary of the modelled flat profiles selected from the two estuaries maximum flow velocities.

Est	Tidal flat	Total length [m]	S_{low} Slope lower flat [−]	S_{up} Slope upper flat [−]	Delta [m]	Velocity [ms^{-1}]
ED	Delfzijl 1	216	1:20	1:2617	10	0.25
ED	Termunterzijl 1	797	1:67	1:680	203	0.13
WS	Paulina 2	429	1:18	1:588	30	0.19
WS	Rilland 1	461	1:63	1:444	77	0.15

the flow velocities on the upper flat reduce towards the dike. In contrast to the profiles WS-Paulina and ED-Delfzijl, the gradient in the velocities during ebb and flood is less pronounced for ED-Termunterzijl and WS-Rilland and the maximum flow velocities are smaller: 0.15 ms^{-1} for WS-Rilland and 0.13 ms^{-1} for ED-Termunterzijl. Compared to the flats with creeks, the flow velocities are 30–40% lower (Table 4). Moreover, the velocities at the lower observation points are higher compared to the flats with creeks.

The flat of ED-Termunterzijl is about 300 m longer compared to other flats. However, the increased water volume that flows over the flat cannot compete with the significant flatter slopes and smaller transition lengths δ of WS-Paulina and ED-Delfzijl., In contrast to WS-Paulina and ED-Delfzijl, the maximum flow velocities at the flat of WS-Rilland occur high in the tidal window because the upper flat lays 1.5 m higher. At this point, the slope of the profile becomes milder. The geometry dominates the flow pattern, friction is less important.
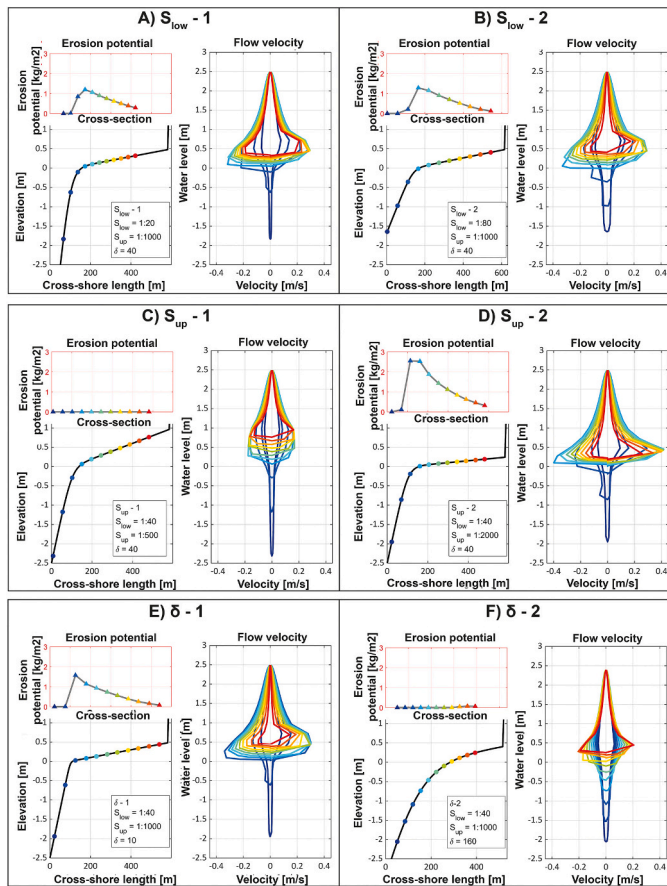
3.2.4. Sensitivity analysis

We performed a sensitivity analysis by varying the flat parameters of the Base case to unravel underlying relations and the effects of the different shape parameters on the flow (Fig. 10). In the different simulations, variations are made for the lower slope (simulations S_{low}-1 and S_{low}-2), the upper slope (simulations S_{up}-1 and S_{up}-2) and the curvature of the transition point (simulations δ-1 and δ-2). With "1" and "2" we denote Variation 1 and Variation 2, respectively. Also, we made one simulation of a concave-up profile. Here, S_{low} and S_{up} where varied both. The flat parameters of each simulation are summarized in Table 5. The curvature was changed by a factor of 4 and the slopes S_{low} and S_{up} were changed by a factor of 2 for each variation.

For each profile, we calculated the erosion potential in addition to the cross-shore flow velocity. When integrating potential erosion over the full tidal cycle (see Eqs. (10)–(12) and Fig. 10), a maximum is found the upper flat close to of the transition. This is a consequence of the local maxima in flow velocities and the long exposure times. The transition point is not only the location where the maximum flow velocities occur. It is also the lowest position of the upper flat, implying that it is part of the upper flat that is longest exposed.

Compared to the Base case, a variation in the lower slope S_{low} does not lead to significant changes in the shape of the velocity profile. This result is in line with the geometrical considerations of the analytical model, which predicts little or no influence of the slope of the lower flat, as long as this lower flat is steeper than the upper flat. The magnitude of the velocity near the transition point increases slightly (by 0.02 ms^{-1}) for S_{low}-2 (Fig. 10A and B). When S_{low} is smaller, the flow velocities increase at the lower part of the tidal flat. This is similar to the profile of WS-Rilland (Fig. 9B). The erosion potential increases slightly for S_{low}-2 because of the slightly larger duration of the high flow velocities. This result is in line with the geometrical considerations of the analytical model, which predicts little or no influence of the slope of the lower flat, as long as this lower flat is steeper than the upper flat.

For simulation S_{up}-1 and S_{up}-2 we steepened and flattened the upper slope, respectively (Fig. 10C and D). In accordance with the predictions of the geometrical model, the magnitude of the velocity is clearly
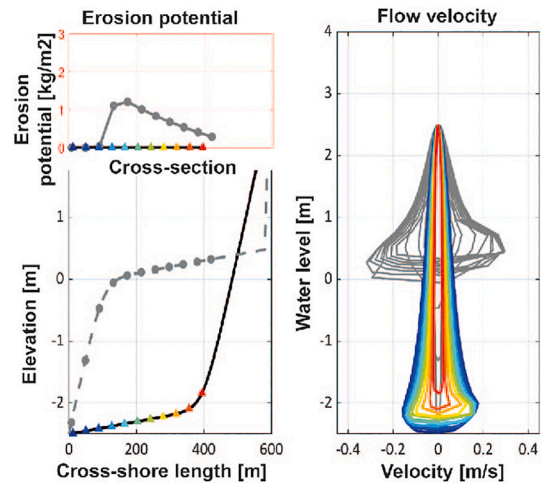
Fig. 10. Variation of profile parameters S_{low}, S_{up} and δ. The simulations with the variations on these parameters are indicated with -1 and the -2. Per simulation we present the flat cross-section including observation points and erosion potential of each observation point (left), velocity profile in each observation point (right).

Fig. 11. Flow velocity and erosion potential of a concave-up tidal flat compared to the Base-case (convex-up) simulation. Left lower panel: the cross-shore profile of the concave-up profile (black) and convex-up (grey) profile. The markers indicate the observation points.

to the Base case (Fig. 7).

The relation between the flow velocity and the curvature of the flat was investigated with simulations δ -1 and δ -2 (Fig. 10E and F). Simulation δ -1 has a sharper transition point compared to the Base case, consequently the change in slope occurs over a smaller distance and is more abrupt. Hence, the water level gradient during ebb flow is larger and the flow velocities increase. The maximum velocity is found during ebb (0.34 ms^{-1}). As a result, the erosion potential increases, especially close to the transition point. The flow velocities higher or lower in the tidal window are hardly affected. In contrast, a larger curvature (δ -2) leads to a reduction of the magnitude of the velocity and the erosion potential. The shape is comparable with the simulation of WS-Rilland (Fig. 9B). The highest flow velocities (0.23 ms^{-1}) occur on the higher part of the tidal flat. In this case, the local slope continues to decrease for higher elevations, and this term dominates the maximum flow velocity.

The analyses in this paper focussed on convex-up profiles of tidal flats because creeks were only observed at flats with such a shape. To illustrate that the occurrence of creeks is generally unlikely on concave-up flats, we show in Fig. 11 the velocity over a concave-up flat with a lower slope of 0.001 [−], δ of 40 [m] and an upper slope of 0.025 [−]. Based on the analytical model (Eq. (9)), the maximum flow velocities occur on the lowest part of the tidal flat where the slope is mildest. In the first part of the flood phase, the flow velocities increase on the lower flat by an linearly with the water level variation. In the transition zone (and above) the increased slope induces a smaller $\frac{\lambda}{d}$ and smaller flow velocities.

affected. In accordance with the predictions of the geometrical model, because the maximum velocity is approximately proportional to the inverse of the upper slope. The shape of the velocity profile remains. The friction effects and the associated slope of the water surface (Fig. 8) are only apparent for a mild upper slope. The asymmetry between ebb and flood flow is much more pronounced for the milder upper slope. Similar to the ED-Delfzijl profile (Fig. 9C), a flood dominant flow is found on the largest part of the upper flat, while the flow becomes ebb dominant at the transition. As a result in simulation S_{up}-1 (steeper slope) the erosion potential does not exceed the critical bed shear stress. In simulation S_{up}-2 (flattened slope) the total effective erosion potential doubles compared

Table 5
Summary of the sensitivity analysis; flat profiles, maximum flow velocities and cumulative bed shear stress.

Est	Tidal flat	Total length m	S_{low} Slope lower flat [−]	S_{up} Slope upper flat [−]	Delta m	Velocity m/s	Erosion potential E_{TM2} [kg/m^2]
–	Base case	600	1:40	1:1000	40	0.32	1.21
–	S_{low} - 1	600	1:20	1:1000	40	0.32	1.20
–	S_{low} - 2	600	1:80	1:1000	40	0.33	1.28
–	S_{up} - 1	600	1:40	1:500	40	0.17	0.00
–	S_{up} - 2	600	1:40	1:2000	40	0.41	2.56
–	δ - 1	600	1:40	1:1000	10	0.34	1.57
–	δ - 2	600	1:40	1:1000	160	0.23	0.07
–	Concave-up	600	1:1000	1:40	40	0.19	0.00

Furthermore, the maximum flow velocities on the concave flat are significantly smaller compared to the Base case (grey velocity profile, Fig. 11). As a result, the erosion potential of the concave tidal flat is negligible. Hence, a convex-up shaped geometry is not favourable for the establishment of creeks.

4. Discussion

4.1. Conceptual framework

Our main aim was to determine where and why creeks are present on tidal flats. Combining the findings of the aerial pictures, tidal flat parameters and model, we found that the tidal flat shape determines the conditions for creek establishment. Creeks develop on convex-up flats with a distinct transition point close to the MWL and a mild slope of the upper flat. The ebb flow is the cause for the development of creeks. The outcomes of the numerical modelling show that three geometry parameters (S_{up}, δ and z_0) and bottom friction affect the cross-shore flow velocity.

The velocity is inversely proportional to the upper slope (S_{up}) of the tidal flat as deduced from the geometric model. A smaller transition zone length (δ) increases the flow velocity. When the water line reaches the transition zone a water level gradient develops. This gradient is enhanced for smaller transition zones, resulting in larger flow velocities. The simulations of the flats in the Ems-Dollard and Western Scheldt and the sensitivity analyses demonstrate the effect of both parameters. Moreover, the parameters increase the ebb dominance at the transition point (Fig. 10). These conclusions are in line with the measurements of Bouma et al. (2005) and the statement of Kleinhans et al. (2009). Finally, when the elevation of the transition point z_0 is close to the MWL, the flow velocities are maximum. Based on the simplified geometric model, it is expected that the elevation of tidal flats affects the maximum current velocity through the water level variation, $\frac{\partial \eta}{\partial t}$, as proven by the geometric model and results of the selected tidal flats. These results are in line with the measurements of Bouma et al. (2005).

The influence of friction has been shown in our study to be a crucial part of the physics. The effect of friction is made explicit by the difference between the numerical model and the geometric model. The latter predicts almost constant current velocities for extended periods of time over the upper flat. In the numerical model the velocity profile is asymmetric and the maximum flow velocities occur during ebb. During ebb, the dewatering of the upper flat is delayed, resulting in a water level gradient close to the transition point and a thin layer of water on the upper flat. Both increase the flow velocity and related erosion potential near the transition point. This coincides with the observation that creeks always intersect the transition point.

Above results indicate where and why creeks develop in the cross shore profile. The precise location of the formation of the creek on a flat in longshore direction is less clearly defined. It will depend on the presence of bed forms and small perturbations, as found in various field studies (Dyer, 1998; Whitehouse et al., 2000; Zhu et al., 2019).

Once a (small) creek/perturbation is initiated as a lower part of the flat, it will attract water. From that moment on, 2D effects will become important. As water is attracted to that location, more water will drain from the flat via that route. This implies, the flow velocities in the creek to be larger compared to the surrounding flat to erode the sediment locally. Without such anomaly or perturbation, the flow conditions in the surrounding area are all uniform. Then this whole zone will erode and a creek will not develop. The presence of creeks leads to a reduction of the flow velocities and bed shear stresses on the adjacent flat. Hence a gradient in flow velocity towards the creek in alongshore direction grows and more water will flow towards the creek, increasing the flow velocity even further. A positive feedback loop is initiated and the creek will grow. This feedback loop was also obtained in the 2D modelling of Xu et al. (2019). The feedback mechanism is likely responsible for the

regular distance as often found between the creeks.

The tidal flats WS-Bath and WS-Paulina have multiple creeks and the spacing between the creeks of WS-Bath is smaller and their cross-sectional area is likely smaller. A similar conclusion can be drawn in the ED when comparing the tidal flat of ED-Delfzijl to ED-Nieuwstad or ED-Bierum. Although not investigated in detail, it is pre-assumable that a smaller cross-sectional area of the creek requests more creeks to discharge an equal volume to satisfy the tidal prism – cross-sectional area relation as studied by D'Alpaos et al. (2010).

The small spacing between creeks also could be a result of the steep upper slope. In the WS, the upper slope of WS-Bath is the steepest of all investigated flats in this study. If the upper slope is steep, less water is "trapped" on the upper flat during ebb flow and the alongshore water level gradient to attract water needs to be larger to compensate the steep upper slope. Hence, an immature creek can only attract water from the direct surrounding which results in a relatively small discharge and flow velocity through the creek. It is most likely that multiple creeks with a small spacing will develop initially. However, in the ED we find less evidence to support this hypothesis. Here the upper flat of ED-Delfzijl has a similar slope compared to the other tidal flats but a smaller creek spacing. This requires more in depth research towards the creek drainage capacity and the tidal flat shape with a 2D model.

4.2. Effect of creeks on flat stability

In this study, the tidal flat shape was a predefined input parameter that was in equilibrium. The hydrodynamic environment and resulting bed shear stresses determine to a large extent the cross-section (Friedrichs, 2011; Friedrichs and Aubrey, 1996). Furthermore, wind waves, sediment type and availability and human interventions also affect the shape of tidal flats (de Vet et al., 2020; Hunt et al., 2015; Kirby, 2000). The cross-section of a tidal flat is in equilibrium if the bed shear stress is uniformly distributed, according to Friedrichs and Aubrey (1996). However, from our model results we conclude that the bed shear stresses are not uniformly distributed and are largest on the upper part near the transition point. Note, however, that these model results do not include the presence of creeks and their influence on the spatial distribution and cross-shore gradients of the bottom shear stress.

We hypothesize that creeks are formed as a consequence of the disequilibrium of the bed shear stress and contribute to the stabilization of a flat morphology that, without creeks, would have too strong gradients in bottom shear stress to persist. To support this hypothesis, we elaborate on the model result qualitatively and only consider the tidal forcing in cross-shore direction. We found peak bed shear stresses near the transition point on the upper slope. This implies that the flat would erode and the transition point will flatten. Simultaneously, the majority of the profiles with creeks was stable. If a creek intersects the tidal flat, it drains part of the water of the surrounding flat and reduces the flow velocities, bed shear stresses and erosion potential near the transition point. If this reduction is sufficient, the transition zone will not erode further. The creeks counteract the initial positive feedback mechanism and can stabilize the shape of the tidal flat.

This suggests that the creeks have impact on the shape of the flats. Predicting the tidal flat shapes in numerical models, would therefore require including the effects of the creeks. Additional research is needed to account for these effects as this is a two-dimensional process. For this, we need high resolution bathymetry information as the creeks can be very narrow compared to the horizontal scales of the flats. Subgrid-based approaches like described in Volp et al. (2016) could be an interesting approach.

Here, we focussed on creeks that develop on the bare part of a fringing tidal flat. We did not investigate creeks that originate in the marsh. Also these creeks have a drainage function (Green and Coco, 2007; Le Hir et al., 2000; Marani et al., 2003a, 2003b) and their influence on the stability of the flat likely depends on the slope of the upper flat. If the upper flat is short and steep, the creek has little influence on

the tidal flat drainage (Le Hir et al., 2000). For long and mild sloped upper flats, the bottom friction becomes significant and drainage via creeks is more efficient. We also did not explicitly consider creeks that were initiated by deposition, as described in (Hood, 2010). Creeks that developed during deposition stages can persist and influence the development of these creek-flat systems.

4.3. Creeks as indicator for profile shapes

We showed that the occurrence of creeks is related to a distinct transition point. This provides the opportunity to get a first estimation of the flat shape in areas where bathymetry data is scarce or even not available. Based on satellite imagery bare tidal flats with and without creeks can be classified. For the flats with creeks, it can be inferred that they have a convex-up shape with a distinct inflection within the zone including creeks (and likely is this elevated close to the MWL).

We observed a variety of creek characteristics on the areal pictures, for example the width and depth of the creek and spacing between creeks. Based on the spatial data and literature (e.g. D'Alpaos et al., 2005), we argue that these creek parameters are correlated to each other and with the flat shape. We hypothesized that creeks with a small distance between them indicate a steeper upper slope.

In both estuaries we found creeks that meander (WS-Paulina) and creeks that are an almost straight line towards the tidal channel (ED-Delfzijl). There is also a variety in bend shape; creeks that have one large bend (ED-Bierum) or multiple smaller bends (WS-Paulina). Kleinhans et al. (2009) found that the strength of the cohesive bed material should be included to evaluate the meander shape of creeks on tidal flats. The meandering is more pronounced on the upper flat compared to the lower flat. This is confirmed by Kleinhans et al. (2009) who found the largest bends near the inflection point. In this area the maximum flow velocities occur on a convex flat (e.g. Fig. 7). Meander migration models relate the bank erosion to the flow velocity in the outer bend (Fagherazzi et al., 2004). Based on the hydrodynamics we expect the largest meanders on the upper flat close to the inflection point. This does not hold for all tidal flats in this study. Inclusion of the sediment properties (e.g. shear strength) can give more insight in the meander behaviour.

4.4. Reliability bathymetry data and model limitations

The high resolution and frequency of the data are a solid base to perform the data analyses. To illustrate the temporal consistency of the tidal flat shape, we plotted the evolution of the cross-section WS-Paulina throughout 2009–2018 (Fig. 12A). Over this period, the shape of the flat remained stable. It indicates that the cross-section of the year 2014 was representative. This was the case for all considered flats, except for the east side of WS-Zuidgors, the flat shape changes and the transition point became more pronounced (Fig. 13). The change of the flat shape is related to dredging and dumping activities as shown by de Vet et al. (2020).

In Fig. 5F, we plotted two profiles of the west side of tidal flat Pauline. The bed level profiles on tidal flat WS-Paulina vary from west to east (Fig. 12B, number 1 most west, number 5 most east). Pronounced double profiles (small δ and large difference between upper and lower slope) are found in the west, while the profiles in the east are less pronounced. Consequently, the creeks developed differently as well. In the west, the creeks are stable over several years. In the east, the creeks have a smaller cross-sectional area, they are shorter and they are less stable over time. These observations coincide with our hypothesis that creeks evolve on flats with a distinct difference between the upper and lower slope and a short transition zone.

The 1D hydrodynamic model schematizes the hydrodynamic processes on a tidal flat. The model was applied to determine the cause of the presence of creeks. This 1D approach is possible as the creeks are oriented in cross-shore direction and this simplified approach allowed for a detailed identification of the relation between velocity, geometry and creek formation potential. Although the model does not explicitly include the bathymetry of the creek, the model captures the relevant hydrodynamic processes for the creek establishment phase.

Alongshore velocities are not considered as a driving force for the creek formation process. First, the alongshore flow results in a transport component perpendicular to the creek (i.e., may rather dampen the formation of creeks). Second, the erosion potential is maximum when the water depth on the upper flat is only a few centimetres (Figs. 7 and 8). Under these conditions, the flow is generally predominantly in
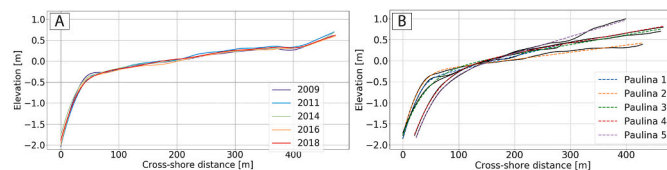

Fig. 12. A) development of cross-section nr. 2 of tidal flat WS-Paulina between 2009 and 2018. B) five cross-sections of tidal flat WS-Paulina from West to East, number 1–5 respectively of 2014.
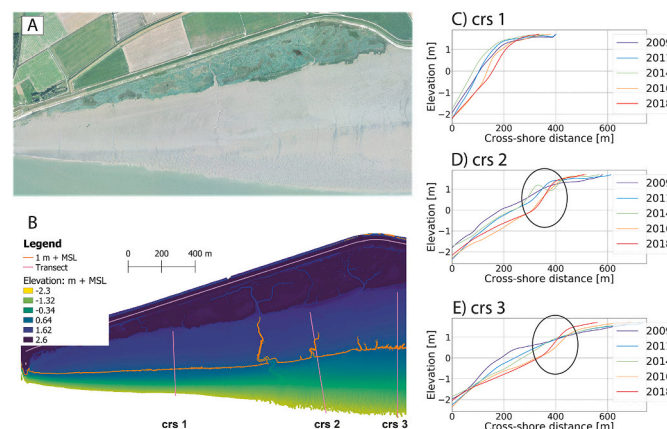

Fig. 13. Spatial variability in profile shape evolution of the WS-Zuidgors flat. A) aerial picture 2014. B) LiDAR 2014. C-E; development of the cross-sections (crs) 1–3 (respectively) for 2009, 2011, 2014, 2016, 2018.

across-flat direction (Le Hir et al., 2000).

Waves are neither considered as a driving process for creek formation (Le Hir et al., 2000) and are therefore not included in the model schematisation, avoiding unnecessary complexity. Convex-up profiles, on which creeks are generally found, are typically tide-dominated in contrast to concave-up tidal flats that are wave-dominated (Friedrichs, 2011). Model studies of tidal flats that include tide and waves show that waves distribute the bed shear stress more gradual on the upper flat (Maan et al., 2018; van der Wegen et al., 2019; van der Wegen et al., 2017). Maan et al. (2018) modelled the 2D flow over a tidal flat including waves, only after waves were excluded in the model. Waves hence likely reduce the possibility of creek formation by damping out these features. However, the LiDAR data and aerial pictures show that creeks persist during successive years and hence overcome storm events. This supports that, at least for the considered flats, creeks do not by default fate away by waves. Hence, our model includes the tidal forcing only.

Sediment characteristics affect the erosion probabilities. In both estuaries the median grain size relates to a broad range of fine grained material. We expect fine sediment on convex tidal flats based on the concept of Friedrichs (2011); the convex shape reduces the wave energy and fine sediment (mud) is found on the surface of the upper tidal flat. This concept corresponds with field measurements on different tidal flats in various estuaries (e.g. Dyer, 1998). The favourable flat shape for creek establishment coincides with the presence of fine grained material. Here, we have not defined a threshold of clay for creek formation. However, we presume that a difference in fine sediment characteristics is of minor importance compared to the flat shape and hydrodynamic conditions.

Furthermore, below this surface layer of sediment, more consolidated material can be found which is less erosive (Dyer, 1998). On the other hand, if a creek forms, the erosion probabilities increase when the creeks attracts more water for increasing depths. A more detailed investigation towards the growth of the creeks is required to elaborate on this mechanism and the relevance of the sediment characteristics.

4.5. Uncertainty in flat characteristics

As deduced from the data, there is a large variety of flat shapes. We distinguished between (1) flats with a sharp transition point close to MWL that are intersected by creeks (e.g., ED-Delfzijl Fig. 5C) and (2) flats with large curvature ($\delta > 50$ m) below or above MWL that are not intersected by creeks (e.g., ED-Termunterzijl Fig. 5D). These results are in agreement with the work of (Dyer et al., 2000; Kleinhans et al., 2009; Whitehouse et al., 2000) who reported creeks on flats with a mild upper and steep lower part. Along a cross-section, creeks are found in a zone starting from the LWL, or slightly higher up on the lower flat, until the upper flat. We did not observe flats with creeks only on the lower flat or only on the upper flat (i.e., they always cover the transition point).

However, the tidal flats of WS-Rilland (Fig. 5I) and WS-Zuidgors (Fig. 5H) do not fit well into one of these two defined groups. Both flats have a distinct upper and lower slope in addition to a large curvature ($\delta > 50$ m) and the elevation of the upper flat is relatively high in relation to the tidal window. Such a high elevation, corresponds to small ebb velocities. This explains, why creeks are not observed here at all.

The dredging activities near WS-Zuidgors influenced the cross-section (Fig. 13 and de Vet et al. (2020)). Especially the eastern part of the flat accreted in recent years. On the western part of WS-Zuidgors (Fig. 13A and B), all creeks have their origin in the marsh or are immature. In the eastern part, immature creeks developed. The shape of the flat in the eastern part, in contrast to the western part (Fig. 13C), is not stable (Fig. 13D and E). In the last decade, the shape has been transitioning due to the extensive accretion of the flats. Now, we can define three slopes in this profile. Therefore, the profile does not fit with Eq. (2). Even for this more complex tidal flat shape, creeks develop on the transition point between the upper flat and the "middle" flat, consistently with the results for the flats with the simpler shapes.

5. Conclusion

Worldwide, we find tidal flats, both with and without tidal creeks cutting through. We investigated where and why creeks develop on bare fringing tidal flats and what the impact of these creeks is.

The presence of creeks on bare fringing tidal flats depends on the cross-sectional profile of the tidal flat. Creeks are found on tidal flats with a distinct convex-up shape, characterized by a small transition zone between the mild-sloped upper flat and steep-sloped lower flat. This transition zone is close to the MWL and the creeks intersect the transition zones. For these conditions, the ebb flow is highest leading to the highest erosion potential at the transition zone. A positive feedback loop develops if creeks are initiated. The creek attracts water from the adjacent flat and the larger depth leads to higher flow velocities than on the adjacent flat. This loop develops until a dynamic equilibrium is reached.

As a consequence of the creek presence, a redistribution of bed shear stress develops, allowing for cross-shore shapes that would not exist without the presence of creeks. The shapes with very flat upper slopes and short transition zones might not have existed without the creeks. Two-dimensional numerical modelling with accounting for the feedback loop is however needed to quantify this.

The presence of the creeks on bare fringing tidal flats is an indication for distinct convex-up bed profiles with mild upper slopes. This insight can be used to characterize a tidal flat from satellite images. Additional enhancements could be further explored, like the relation between the distances between creeks and bed slope or the meandering intensity on height and bed slope.

Declaration of competing interest

The authors declare that they have no known competing financial interests or personal relationships that could have appeared to influence the work reported in this paper.
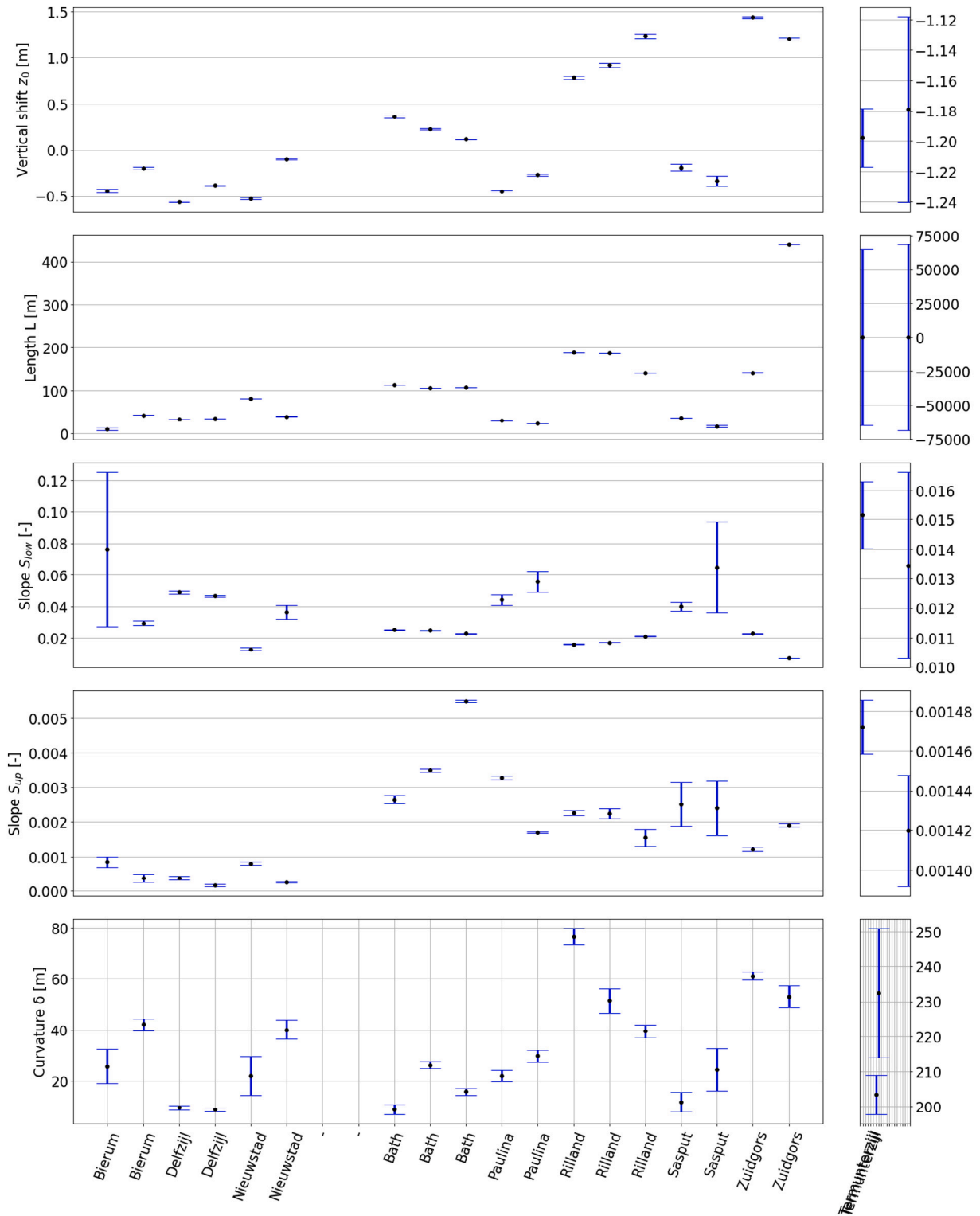
Appendix A

[Appendix-Table A](#) presents the profile properties of each cross-section per tidal flat in both estuaries. The total flat lengths vary between 190 and 820 m in both estuaries. In general, the length L is less than $1/3$ of the total flat length. At flats with multiple creeks present, the spacing between creeks varies between 20 and 1000 m and often the creeks end close to the low water line (LWL).

Appendix-Table A
Profile properties.

Estuary	locations	Creeks	Creek start; offset from LWL [m]	Creek length [m]	Spacing between creeks [m]	Total length [m]	Length lower flat [m]	Length upper flat [m]	S_{low} Slope lower flat [−]	S_{up} Slope upper flat [−]	δ Delta [m]
ED	Bierum 1	Yes	20	190	–	247.28	10.29	236.99	7.62E-02	8.49E-04	25.73
ED	Bierum 2	Yes	–	–	–	191.07	43.03	148.04	2.93E-02	3.76E-04	42.20
ED	Delfzijl 1	Yes	0	125	20–70	216.41	33.68	182.73	4.89E-02	3.82E-04	9.55
ED	Delfzijl 2	Yes	0	125	20–70	198.76	35.21	163.55	4.65E-02	1.74E-04	8.77
ED	Nieuwstad 1	Yes	0	230	300–1000	493.99	81.12	412.88	1.28E-02	8.04E-04	22.09
ED	Nieuwstad 2	Yes	25	410	300–1000	622.95	40.11	582.84	3.64E-02	2.54E-04	40.15
ED	Termun-terzijl 1	No	–	–	–	797.30	0.00	797.30	1.52E-02	1.47E-03	203.36
ED	Termun-terzijl 2	No	–	–	–	818.81	0.00	818.81	1.35E-02	1.42E-03	232.42
WS	Bath 1	Yes	70	180	30	234.77	112.77	122.00	2.52E-02	2.65E-03	8.85
WS	Bath 2	Yes	70	140	30	333.35	106.48	226.87	2.49E-02	3.49E-03	26.27
WS	Bath 3	Yes	60	130	30	347.73	107.79	239.94	2.28E-02	5.49E-03	15.88
WS	Paulina 1	Yes	0	190	80–150	286.08	30.83	255.18	4.42E-02	3.28E-03	21.97
WS	Paulina 2	Yes	0	155	80–150	429.28	23.85	405.23	5.57E-02	1.70E-03	29.75
WS	Rilland 1	No	–	–	–	461.28	188.28	273.00	1.60E-02	2.25E-03	76.66
WS	Rilland 2	No	–	–	–	421.61	186.47	235.14	1.71E-02	2.24E-03	51.47
WS	Rilland 3	No	–	–	–	264.21	140.30	123.92	2.11E-02	1.55E-03	39.54
WS	Sasput 1	Yes	0	80	30–120	117.36	36.70	80.65	4.00E-02	2.51E-03	11.92
WS	Sasput 2	Yes	0	80	30–120	124.25	17.10	107.15	6.48E-02	2.39E-03	24.48
WS	Zuidgors 1	Yes	–	–	–	367.22	141.45	225.76	2.28E-02	1.22E-03	61.17
WS	Zuidgors 2	Yes	390	410	100–250	722.33	440.14	282.19	7.05E-03	1.89E-03	53.11

The mean values and standard deviation of the profile parameters are visualized in [Appendix-Fig. A](#). We separated the results of ED-Termunterzijl (right panel) from the other eight tidal flats (left panel). For the flats of the left panel, we can conclude that the standard deviations of z_0, S_{low}, S_{up} and δ and L are small. For ED-Bierum, WS-Sasput and ED-Nieuwstad the standard deviations of S_{low}, S_{up} and δ increase slightly due to the fact that the upper part of the tidal flat is not level. For the flat ED-Termunterzijl, it is possible to find parameters that result in an apparently well fit when considering, panel ED-Termunterzijl. The mean values vary significantly compared to the other tidal flats. Moreover the standard deviations are significant. For these kind of profiles, δ is large and L becomes zero, hence the profile is not double sloped.

Appendix-Fig. A. Mean values and standard deviations of profile parameters.

References

Bouma, T.J., De Vries, M.B., Low, E., Kusters, L., Herman, P.M.J., Tánczos, I.C., Van Regenmortel, S., 2005. Flow hydrodynamics on a mudflat and in salt marsh vegetation: Identifying general relationships for habitat characterisations. Hydrobiologia 540 (1–3), 259–274. https://doi.org/10.1007/s10750-004-7149-0.

Casulli, V., 2009. A high-resolution wetting and drying algorithm for free-surface hydrodynamics, 60, 391–408. https://doi.org/10.1002/fld.1896.

Coco, G., Zhou, Z., van Maanen, B., Olabarrieta, M., Tinoco, R., Townend, I., 2013. Morphodynamics of tidal networks: advances and challenges. Mar. Geol. 346, 1–16. https://doi.org/10.1016/j.margeo.2013.08.005.

Compton, T.J., Holthuijsen, S., Mulder, M., van Arkel, M., Schaars, L.K., Koolhaas, A., van der Veer, H.W., 2017a. Shifting baselines in the Ems Dollard estuary: a

comparison across three decades reveals changing benthic communities. J. Sea Res. 127 (June), 119–132. https://doi.org/10.1016/j.seares.2017.06.014.

Compton, T.J., Holthuijsen, S., Mulder, M., van Arkel, M., Schaars, L.K., Koolhaas, A., van der Veer, H.W., 2017b. Shifting baselines in the Ems Dollard estuary: a comparison across three decades reveals changing benthic communities. J. Sea Res. 127 (June), 119–132. https://doi.org/10.1016/j.seares.2017.06.014.

D'Alpaos, A., Lanzoni, S., Marani, M., Fagherazzi, S., Rinaldo, A., 2005. Tidal network ontogeny: channel initiation and early development. J. Geophys. Res. Earth Surf. 110 (2), 1–14. https://doi.org/10.1029/2004JF000182.

D'Alpaos, A., Lanzoni, S., Marani, M., Rinaldo, A., 2010. On the tidal prism-channel area relations. Journal of Geophysical Research: Earth Surface 115 (1), 1–13. https://doi.org/10.1029/2008JF001243.

Dam, G., van der Wegen, M., Roelvink, D., 2013. Coastal Dynamics 2013 Long-term performance of process-based models in estuaries. In: Proceedings of Coastal Dynamics, pp. 409–420.

[dataset] DINOloket, 2021. Partical Size Distribution Delfzijl, Bierum, Nieuwstad. Retrieved June 22. https://www.dinoloket.nl/ondergrondgegevens.

Dyer, K.R., 1998. In: The Typology of Intertidal Mudflats, 139. Geological Society Special Publication, pp. 11–24. https://doi.org/10.1144/GSL.SP.1998.139.01.02.

Dyer, K.R., Christie, M.C., Wright, E.W., 2000. The classification of intertidal mud # ats. Cont. Shelf Res. 20 (January), 1039–1060.

Fagherazzi, S., Mariotti, G., 2012. Mudflat runnels: evidence and importance of very shallow flows in intertidal morphodynamics. Geophys. Res. Lett. 39 (14), 1–6. https://doi.org/10.1029/2012GL052542.

Fagherazzi, Sergio, Gabet, E.J., Furbish, D.J., 2004. The effect of bidirectional flow on tidal channel planforms. Earth Surf. Process. Landf. 29 (3), 295–309. https://doi.org/10.1002/esp.1016.

Friedrichs, C.T., 2011. Tidal flat morphodynamics: a synthesis. In: Treatise on Estuarine and Coastal Science, 3. https://doi.org/10.1016/B978-0-12-374711-2.00307-7.

Friedrichs, C.T., Aubrey, D.G., 1996. In: Uniform Bottom Shear Stress and Equilibrium Hyposometry of Intertidal Flats. (January 1996), pp. 405–429. https://doi.org/10.1029/ce050p0405.

Friedrichs, Carl T., Madsen, O.S., 1992. Nonlinear diffusion of the tidal signal in frictionally dominated embayments. J. Geophys. Res. 97 (C4), 5637. https://doi.org/10.1029/92jc00354.

[dataset] Google Earth Pro, 2016. [Google Earth 2016 10 m]. Retrieved Feb 12, 2021 [dataset].

Green, M.O., Coco, G., 2007. Sediment transport on an estuarine intertidal flat: Measurements and conceptual model of waves, rainfall and exchanges with a tidal creek. Estuar. Coast. Shelf Sci. 72 (4), 553–569. https://doi.org/10.1016/j.ecss.2006.11.006.

Herrling, G., Elsebach, J., Ritzgmann, A., 2014. Evaluation of changes in the tidal regime of the Ems-Dollard and lower Weser estuaries by mathematical modelling. Kuste 81, 353–368.

Hood, W.G., 2010. Tidal channel meander formation by depositional rather than erosional processes: examples from the prograding Skagit River Delta (Washington, USA). Earth Surf. Process. Landf. 35 (3), 319–330. https://doi.org/10.1002/esp.1920.

Hunt, S., Bryan, K.R., Mullarney, J.C., 2015. The influence of wind and waves on the existence of stable intertidal morphology in meso-tidal estuaries. Geomorphology 228, 158–174. https://doi.org/10.1016/j.geomorph.2014.09.001.

Kirby, R., 2000. Practical implications of tidal flat shape. Cont. Shelf Res. 20 (10–11), 1061–1077. https://doi.org/10.1016/S0278-4343(00)00012-1.

Kleinhans, M.G., Schuurman, F., Bakx, W., Markies, H., 2009. Meandering channel dynamics in highly cohesive sediment on an intertidal mud flat in the Westerschelde estuary, the Netherlands. Geomorphology 105 (3–4), 261–276. https://doi.org/10.1016/j.geomorph.2008.10.005.

Le Hir, P., Roberts, W., Cazaillet, O., Christie, M., Bassoullet, P., Bacher, C., 2000. Characterization of intertidal flat hydrodynamics. Cont. Shelf Res. 20 (12–13), 1433–1459. https://doi.org/10.1016/S0278-4343(00)00031-5.

Maan, D.C., van Prooijen, B.C., Zhu, Q., Wang, Z.B., 2018. Morphodynamic feedback loops control stable fringing flats. J. Geophys. Res. Earth Surf. 123 (11), 2993–3012. https://doi.org/10.1029/2018JF004659.

Marani, M., Belluco, E., D'Alpaos, A., Defina, A., Lanzoni, S., Rinaldo, A., 2003. On the drainage density of tidal networks. Water Resour. Res. 39 (2), 1–11. https://doi.org/10.1029/2001WR001051.

Marani, M., Silvestri, S., Belluco, E., Camuffo, M., D'Alpaos, A., Lanzoni, S., Rinaldo, A., 2003. Patterns in tidal environments: Salt-marsh channel networks and vegetation. Int. Geosci. Remote Sens. Symp. 5 (1), 3269–3271. https://doi.org/10.1109/igarss.2003.1294752.

[dataset] Province of Zeeland, 2014. Zeeland 2014 25 cm. Retrieved Feb 12, 2021. https://kaarten.zeeland.nl/map/cultuurhistorie.

QGIS.org, 2021. QGIS Development Team (2021). QGIS Geographic Information System. Open Source Geospatial Foundation Project. http://qgis.osgeo.org.

RWS, 2014. LiDAR data [hoogte 2014 2m]. Retrieved Nov 5 2018. https://www.rijkswaterstaat.nl/apps/geoservices/geodata/dmc/hoogte_2014/.

RWS Waterinfo, 2014. Waterlevel data of stations: Delfzijl, Eemshaven, Nieuwstatenzijl, Bath, Breskensveerhaven, Terneuzen. Retrieved May 18 2020. https://waterinfo.rws.nl/?#!/nav/bulkdownload/huidige-selectie/.

Stark, J., Smolders, S., Meire, P., Temmerman, S., 2017. Impact of intertidal area characteristics on estuarine tidal hydrodynamics: a modelling study for the Scheldt Estuary. Estuar. Coast. Shelf Sci. 198, 138–155. https://doi.org/10.1016/j.ecss.2017.09.004.

Talke, S.A., De Swart, H.E., De Jonge, V.N., 2009. An idealized model and systematic process study of oxygen depletion in highly turbid estuaries. Estuar. Coasts 32 (4), 602–620. https://doi.org/10.1007/s12237-009-9171-y.

de Vet, P.L.M., van Prooijen, B.C., Wang, Z.B., 2017. The differences in morphological development between the intertidal flats of the Eastern and Western Scheldt. Geomorphology 281, 31–42. https://doi.org/10.1016/j.geomorph.2016.12.031.

de Vet, P.L.M., van Prooijen, B.C., Colosimo, I., Ysebaert, T., Herman, P.M.J., Wang, Z.B., 2020. Sediment disposals in estuarine channels alter the eco-morphology of intertidal flats. J. Geophys. Res. Earth Surf. 125 (2) https://doi.org/10.1029/2019JF005432.

Volp, N.D., Van Prooijen, B.C., Stelling, G.S., 2013. A finite volume approach for shallow water flow accounting for high-resolution bathymetry and roughness data. Water Resour. Res. 49 (7), 4126–4135. https://doi.org/10.1002/wrcr.20324.

Volp, N.D., van Prooijen, B.C., Pietrzak, J.D., Stelling, G.S., 2016. A subgrid based approach for morphodynamic modelling. Adv. Water Resour. 93, 105–117. https://doi.org/10.1016/j.advwatres.2015.07.013.

Wang, Z.B., Vandenbruwaene, W., Taal, M., Winterwerp, H., 2019. Amplification and deformation of tidal wave in the Upper Scheldt Estuary. Ocean Dyn. 69 (7), 829–839. https://doi.org/10.1007/s10236-019-01281-3.

Weerman, E.J., Koppel van den, J., Eppinga, M.B., Montserrat, F., Liu, Q.-X., Herman, P.M.J., 2010. Spatial self-organization on intertidal mudflats through biophysical stress divergence. Am. Nat. 176, E15–E32. https://doi.org/10.1086/652991.

van der Wegen, M., Roelvink, J.A., 2012. Reproduction of estuarine bathymetry by means of a process-based model: Western Scheldt case study, the Netherlands. Geomorphology 179, 152–167. https://doi.org/10.1016/j.geomorph.2012.08.007.

van der Wegen, Mick, Jaffe, B., Foxgrover, A., Roelvink, D., 2017. Mudflat morphodynamics and the impact of sea level rise in South San Francisco Bay. Estuar. Coasts 40 (1), 37–49. https://doi.org/10.1007/s12237-016-0129-6.

van der Wegen, M., Roelvink, J.A., Jaffe, B.E., 2019. Morphodynamic resilience of intertidal mudflats on a seasonal time scale. J. Geophys. Res. Oceans 124 (11), 8290–8308. https://doi.org/10.1029/2019JC015492.

Whitehouse, R.J.S., Bassoullet, P., Dyer, K.R., Mitchener, H.J., Roberts, W., 2000. The influence of bedforms on flow and sediment transport over intertidal mudflats. Cont. Shelf Res. 20 (10–11), 1099–1124. https://doi.org/10.1016/S0278-4343(00)00014-5.

Willemsen, P.W.J.M., Borsje, B.W., Hulscher, S.J.M.H., Van der Wal, D., Zhu, Z., Oteman, B., Bouma, T.J., 2018. Quantifying bed level change at the transition of Tidal flat and Salt Marsh: can we understand the lateral location of the Marsh Edge? J. Geophys. Res. Earth Surf. 123 (10), 2509–2524. https://doi.org/10.1029/2018JF004742.

Winterwerp, J.C., Van Kesteren, W.G.M., 2004. Introduction to the Physics of Cohesive Sediment Dynamics in the Marine Environment. Elsevier.

Xie, W., He, Q., Wang, X., Guo, L., Zhang, K., 2018. Role of mudflat-creek sediment exchanges in intertidal sedimentary processes. J. Hydrol. 567 (October), 351–360. https://doi.org/10.1016/j.jhydrol.2018.10.027.

Xu, F., Coco, G., Zhou, Z., Tao, J., Zhang, C., 2017. A numerical study of equilibrium states in tidal network morphodynamics. Ocean Dyn. 67 (12), 1593–1607. https://doi.org/10.1007/s10236-017-1101-0.

Xu, F., Coco, G., Tao, J., Zhou, Z., Zhang, C., Lanzoni, S., D'Alpaos, A., 2019. On the morphodynamic equilibrium of a short tidal channel. J. Geophys. Res. Earth Surf. 124 (2), 639–665. https://doi.org/10.1029/2018JF004952.

Ysebaert, T., Herman, P.M.J., Meire, P., Craeymeersch, J., Verbeek, H., Heip, C.H.R., 2003. Large-scale spatial patterns in estuaries: estuarine macrobenthic communities in the Schelde estuary, NW Europe. Estuar. Coast. Shelf Sci. 57 (1–2), 335–355. https://doi.org/10.1016/S0272-7714(02)00359-1.

Zhou, Z., Stefanon, L., Olabarrieta, M., D'Alpaos, A., Carniello, L., Coco, G., 2014. Analysis of the drainage density of experimental and modelled tidal networks. Earth Surf. Dyn. 2 (1), 105–116. https://doi.org/10.5194/esurf-2-105-2014.

Zhu, Q., van Prooijen, B.C., Maan, D.C., Wang, Z.B., Yao, P., Daggers, T., Yang, S.L., 2019. The heterogeneity of mudflat erodibility. Geomorphology 345. https://doi.org/10.1016/j.geomorph.2019.106834.